Journal of Enhanced Heat Transfer, 26(2):101–126 (2019)

HEAT TRANSFER AND PRESSURE DROP CHARACTERISTICS FOR FLOW THROUGH SQUARE CHANNEL WITH DELTA WING VORTEX GENERATOR ELEMENTS ON TWO OPPOSITE WALLS

M.K. Nalawade,[1,] A. Bhati,[2] & R.P. Vedula[2]*

[1]*Vishwarma Institute of Technology, Pune, India*

[2]*Department of Mechanical Engineering, Indian Institute of Technology, Bombay, India*

*Address all correspondence to: M.K. Nalawade, Vishwarma Institute of Technology, Pune, India; Tel.: +912024202148, E-mail: mukundnalawade@gmail.com

Original Manuscript Submitted: 10/15/2017; Final Draft Received: 9/14/2018

Experimental results for friction factor and heat transfer coefficients for flow through a square duct with delta wing vortex generators on two opposite walls are reported. The effects of geometrical parameters such as pitch-to-height ratio, aspect ratio, and height-to-duct hydraulic diameter ratio on the heat transfer coefficient and pressure drop were studied. Comprehensive results for a single vortex generator and limited data for two vortex generators in the spanwise direction at a given axial location are presented. Detailed local heat transfer distributions are presented for selected configurations. High heat transfer coefficients were observed both underneath and between successive vortex generator elements. The magnitudes of average heat transfer coefficients on the smooth walls adjacent to the roughened walls were only about 10% lower than those for the roughened walls. The ratio of Nusselt number and friction factor with and without the delta wing vortex generators for constant Reynolds number conditions are presented. The Nusselt number ratios at constant pumping power condition are also reported; the highest values for a single and two vortex generators at an axial location were observed to be 2.8 and 3.1, respectively. Semi-empirical correlations for heat transfer and friction factor, developed on the basis of available methodologies for roughened ducts, predict the measured data to within an error of about 15%.

KEY WORDS: *heat transfer enhancement, Delta Wing, vortex generators, internal flow*

1. INTRODUCTION

Several techniques have been used to enhance heat transfer coefficients in internal flows, such as appropriately shaped inserts known as Vortex Generators (VGs). The longitudinal vortices created by these devices promote mixing in the flow field, resulting in enhanced heat transfer coefficients. Edwards and Alker (1974) studied the use of longitudinal vortices to enhance heat transfer on flat surfaces. Their experimental results for cubes and delta winglet VGs in a fully developed duct flow revealed a maximum local Nusselt number enhancement of about 76%.

NOMENCLATURE

A	area of heated wall (m^2)	$\text{Nu}_{sa,r}(x)$	spanwise average Nusselt number for roughened walls, Eq. (3b)
b	span of VG (m)	$\text{Nu}_{sa,s}(x)$	spanwise average Nusselt number for smooth walls, Eq. (3b)
c	chord length of VG (m)	Nu_{ss}	overall averaged Nusselt number for smooth walls, Eq. (3c)
c_p	specific heat of fluid (Air) (J/kg-K)	Nu_L	local Nusselt number at location (x, y, z), Eq. (3a)
D_h	hydraulic mean diameter of test section (m)	p	pitch of VGs (m)
e	height of VG tip above the surface of roughened wall (m)	Δp	pressure drop in the test section (Pa)
e^+	roughness Reynolds number, $e^+ = (e/D_h)(f_r/2)^{1/2}\text{Re}$	Pr	Prandtl number, $\mu c_P/k$
f	friction factor in a channel with opposite two walls roughened	q	heat flux (W/m^2-K)
f_c	friction factor in a smooth channel for the effective Reynolds number (Rec)	Re	Reynolds number, $\rho\overline{V}D_h/\mu$
f_r	friction factor for four-sided roughened channel	Rec	effective Reynolds number for constant pumping power, Eq. (5)
f_s	friction factor in channel with all smooth sides	$R(e^+)$	roughness function for friction
G	heat transfer roughness function	St_{4r}	stanton number for flow in a channel with four roughened walls, Nu/(Re.Pr)
H	height of the channel (m)	$T_b(x)$	bulk temperature at a streamwise location x (K), Eq. (3d)
k	thermal conductivity of the fluid (air), (W/m-K)	$T_w(x, y, z)$	wall temperature at a location x, y, z (K)
L	test section length	$\overline{V}$	average velocity (m/s)
Li	axial location for local Nu plot, $i = 2$ to 9	W	width of channel (m)
$\dot{m}$	mass flow rate (kg/s)	x	streamwise direction coordinate (m)
Nu_{rr}	overall averaged Nusselt number for roughened walls, Eq. (3c)	y	axial distance along breadth of channel from centerline (m)
Nu_a	average Nusselt number over all four walls of the channel	z	axial distance along width of channel from centerline (m)
Nu_c	Nusselt number for smooth channel on basis of equal pumping power	**Greek Symbols**	
Nu_s	Nusselt number for smooth channel on basis of equal Reynolds number	β	angle of attack of VG, $\sin^{-1}[(\Lambda/2).(e/D_h)]$
		Λ	aspect ratio of delta wing VG, $2b/c$
		μ	dynamic viscosity, (Pa-s)
		ρ	density (kg/m^3)

Turk and Junkhan (1986) reported an overall heat transfer enhancement of 25%–50% by using rectangular wings on a flat plate. Fiebig et al. (1986) reported local measurement of heat transfer for delta wing and delta winglet pair VGs in a rectangular channel with Reynolds numbers between 1360 and 2270, and observed a maximum heat transfer enhancement of 60%. Fiebig et al. (1991) reported experimental results with longitudinal VGs in a channel flow for $1000 \leq \mathrm{Re} \leq 2000$ for a single delta wing, rectangular wing, and a single pair of delta or rectangular winglets for angles of attack between 10° and 60°. Delta wings were the most effective for heat transfer enhancement per unit increase in friction drop. The heat transfer coefficients were increased by up to 50%–77% and the maximum pressure drop increase was approximately 45%. Fiebig et al. (1993) studied the effect of delta wing VGs on heat transfer inside a fin and tube heat exchanger, and reported a 55%–65% increase in heat transfer coefficient values.

Han et al. (1994) reported heat transfer coefficient data for delta-shaped solid ribs located inside a square channel. The backward delta shaped in-line rib configuration produced the highest increase in the heat transfer. Wang et al. (2002a) reported flow visualization results for the effects of VGs in a fin and tube heat exchanger for laminar flow with Reynolds numbers in the range of 500–2500. Jacobi and Shah (1995) presented a review of the progress in heat transfer enhancement using longitudinal VGs, and suggested further studies on parametric variation of geometric and flow conditions. Tiggelbeck et al. (1992) investigated flow structure and heat transfer inside a rectangular channel using two rows of delta winglets (three pairs of delta winglets in each row) in aligned geometry, keeping winglet aspect ratio of 2 and angle of attack of 45°. The local heat transfer enhancement behind the second row of VGs was higher than that behind the first row. A 77% increase in average heat transfer and a 460% increase in the local heat transfer behind the second row had a Reynolds number of 5600, and pitch-to-channel height ratio equal to 7. The effect of staggering the winglets and variable angle of attack for first and second row of winglets caused the inline configuration to be slightly better than the staggered one reported by Tiggelbeck et al. (1993). They reported an optimal angle of attack of 55° for the first row and 70° for the second row of winglets, and a mean heat transfer enhancement of 80% at Reynolds number equal to 6000.

Gentry and Jacobi (1997) reported a 50%–60% heat transfer enhancement over a flat plate using delta wings, and in 2002 presented detailed heat transfer and pressure drop results for delta wings placed at the leading edge of a flat plate for laminar flow. A 300% increase in local heat transfer coefficients over the baseline case was reported. The largest spatially averaged heat transfer enhancement equal to 55% was at an angle of attack and aspect ratio equal to 55° and 2, respectively, which was accompanied by a 100% increase in the pressure drop with respect to the smooth case. Joardar and Jacobi (2005) studied the effect of delta wing VGs on a flat tube, louvered-fin compact heat exchanger and found a 21% increase in the overall heat transfer performance. Wang et al. (2002b) reported the heat transfer performance with delta winglet type Vortex Generators mounted on the fin surface of a bank of flat heat exchanger tubes. The VGs provided significant enhancement over the fin surface, both close to the flat tube as well as in the downstream region.

Biswas and Chattopadhyay (1992) conducted numerical studies to compare the effect of stamping of delta wing VGs using a single VG for a channel aspect ratio, delta wing aspect ratio, angle of attack, and Reynolds number equal to 2, 1, 26°, and 500, respectively. Augmentations in the heat transfer at the channel exit for nonstamped and stamped cases were equal to 34% and 10%, respectively. A 79% increase in friction factor for nonstamped delta wing VGs was about 48% higher than the friction factor for stamped VG case. Detailed computational results by Biswas et al. (1996) for the flow structure and enhancement mechanism in a channel with a

single built-in winglet type VG for laminar flow revealed an enhancement of 65% for an angle of attack of 37.5°, aspect ratio of 3, and Reynolds number equal to 1580. Numerical simulations (Zhu et al., 1993) for four basic forms of VGs in a developing turbulent channel flow results in overall heat transfer enhancement of 16%, 16.5%, 17%, and 19% for rectangular wings, delta wings, rectangular winglet pairs, and delta winglet pairs, respectively, for Reynolds number equal to 50,000 and angle of attack equal to 25°. The location of the vortex depended on the size and geometry of VG, and to get heat transfer enhancement, it was more useful to generate a vortex near the wall to disturb the laminar sublayer.

Fiebig et al. (1989) performed numerical calculations for developing laminar flow between parallel flat plates with 10 delta wings at a pitch-to-channel height ratio of 2, an aspect ratio of unity. and an angle of attack between 10° and 50° for $500 < \mathrm{Re} < 4000$ (Re based on channel height). An absence of vortex breakdown was seen until an angle of attack of 50°; local heat transfer enhancements were as high as 300% at this angle of attack and $\mathrm{Re} = 4000$ when compared to the plane channel case. A numerical study (Hu et al., 2013) for the determination of the optimal spacing between fins with vortex generators using the area goodness factor as the parameter for finned tube heat exchangers showed change in optimal fin spacing for changing inlet velocity, keeping inlet area and flow rate same. Wu and Tao (2012) investigated, numerically and experimentally, the influence of a pair of delta winglet vortex generators on the heat transfer and flow characteristics at low Reynolds numbers (less than 2000). The largest angle of attack at 60° resulted in the largest heat transfer enhancement equal to about 1.5 times the channel without the vortex generator.

Tang et al. (2016) proposed the use of an additional elliptical pole element to delta wing and rectangular wing vortex generators and reported numerical results for heat transfer enhancement. The maximum enhancement in heat transfer coefficient was 30% over the no vortex generator case and a maximum performance evaluation factor at constant pumping power equal to 1.1 was calculated. Lei et al. (2017) studied the influence of inserting a tape with delta winglet VGs punched in it to enhance the heat transfer characteristics. The performance evaluation criterion index based on the constant pumping power criterion was reported to be highest and equal to about 1.35 for the lowest angle of attack ($= 15°$) at very low Reynolds numbers (about 5000) and reduced to about 1.2 at high Reynolds numbers (about 20,000).

Liou et al. (2000) investigated heat transfer enhancement in a square duct with 12 different shaped VGs at a single $\mathrm{Re} = 12{,}000$. They reported the highest pitch averaged Nusselt number augmentation of 2.5 under the constant pumping power criteria for normal delta wings and block shaped delta wings. Akbari et al. (2009) reported local heat transfer coefficient data of delta winglet pair vortex generators positioned in rectangular channel with a large aspect ratio. The vortex generator elements altered the wake region downstream of the tubes and the flow Reynolds number based on twice the channel height was kept below 2000. Qi et al. (2010) reported heat transfer data for a longitudinal vortex generator that was a combination of two rectangular vortex generators. The optimum performance was obtained by using a 30° orientation compared to the 45° that is normally observed for simple VGs. Bekele et al. (2011) studied the overall heat transfer augmentation by delta wing VGs for a rectangular duct with aspect ratio of 6. The VGs were mounted on one wall of the duct at an angle of attack equal to 90°. A thermohydraulic performance enhancement of 2.1 was reported for a longitudinal pitch to height of VG ratio equal to 5.5, height of VG to channel height ratio equal to 0.5, and Reynolds number equal to 10,000. Bekele et al. (2014) extended their earlier study to include more geometrical parameters for the VGs over a wider Reynolds number range for the same rectangular channel geometry and reported a thermohydraulic performance as high as 3.89 for selected parameters.

Skullong and Promvonge (2014) reported the use of delta wing type VGs on one wall of a channel with aspect ratio 10, for heat transfer enhancement. The overall surface average heat transfer coefficients were reported, with the maximum enhancement ratio for constant pumping power criterion being equal to 2.15. Eimsa-ard and Promvongue (2011) studied the use of punched delta wing vortex generators for heat transfer enhancement. The delta wings facing in the forward and backward direction in straight tapes as well as tapes with axis twist were investigated for several geometric parameters; the maximum performance enhancement factor was about 1.3 at low Reynolds number (about 4000). Caliskan (2014) studied the effect of punched triangular and rectangular VGs inside a channel using five rows of punched VGs at different channel heights, and a pitch to channel width ratio of 0.2 for varying base of VG to base of channel ratio and angle of attack; maximum thermal enhancement factors were 2.92 and 2.90 with punched triangular and rectangular VGs, respectively.

A plane tape insert with delta wing vortex generators cut out in it for heat transfer enhancement in a tube was studied by Skullong et al. (2016). Using several angles of attack, the Nusselt number enhancement was as high as 500%. The constant pumping power enhancement for the insert was shown to be better than that for coiled wire and twisted tape inserts. Chamoli et al. (2017) used curved delta wing vortex generators attached to the wall of a tube for increased heat transfer coefficients and perforated them to reduce pressure drop. Several parameters were studied; the thermal enhancement factor was as high as 1.65. Numerical studies by Xu et al. (2018) for several vortex generator shapes revealed that a semi-cylindrical shape was best, based on constant pumping power criterion. Several computations to study the heat transfer and friction factor characteristics for varying length, diameter, and spacing for an inline configuration were presented. Lemenand et al. (2018) studied the flow distribution in a channel with a single trapezoidal vortex generator. The heat transfer coefficient peaked at the location where the vortex generator is attached to the wall. The Nusselt number was reported to drop much more rapidly compared to the vorticity field.

The above literature indicates that most studies on the use of multiple VGs for heat transfer enhancement are restricted to plane wall external flow or internal flows with high aspect ratio ducts with VGs on one wall only. In addition, local spatially resolved heat transfer coefficient measurements are available only for very few configurations. The present study reports local heat transfer coefficient measurements for a square cross-section channel with delta wing VGs on two opposite walls for a wide range of geometric parameters of the delta wing VGs. Limited data for VGs on one, two, or four walls are presented. However, VGs on two opposite walls were studied in detail because they give the best heat transfer performance at constant pumping power, in addition to smaller overall pressure drop. Semi-empirical correlations for heat transfer coefficient and pressure drop are presented, using the analysis methodology reported by Han et al. (1984, 1988). The use of delta wing vortex generators is useful for providing mixing close to the surface on which they are mounted and result in high heat transfer coefficient values both at constant Reynolds numbers and constant pumping power conditions. Manufacturing constraints were not considered in the current study.

2. METHODS

A schematic of the experimental set-up is shown in Fig. 1. Air from a blower enters the test section through a calibrated venturimeter. The pressure difference across the inlet and throat sections of the venturimeter, and absolute pressure at the throat section, measured by U-tube manometers with water as the working fluid, were used for computation of mass flow rate through the

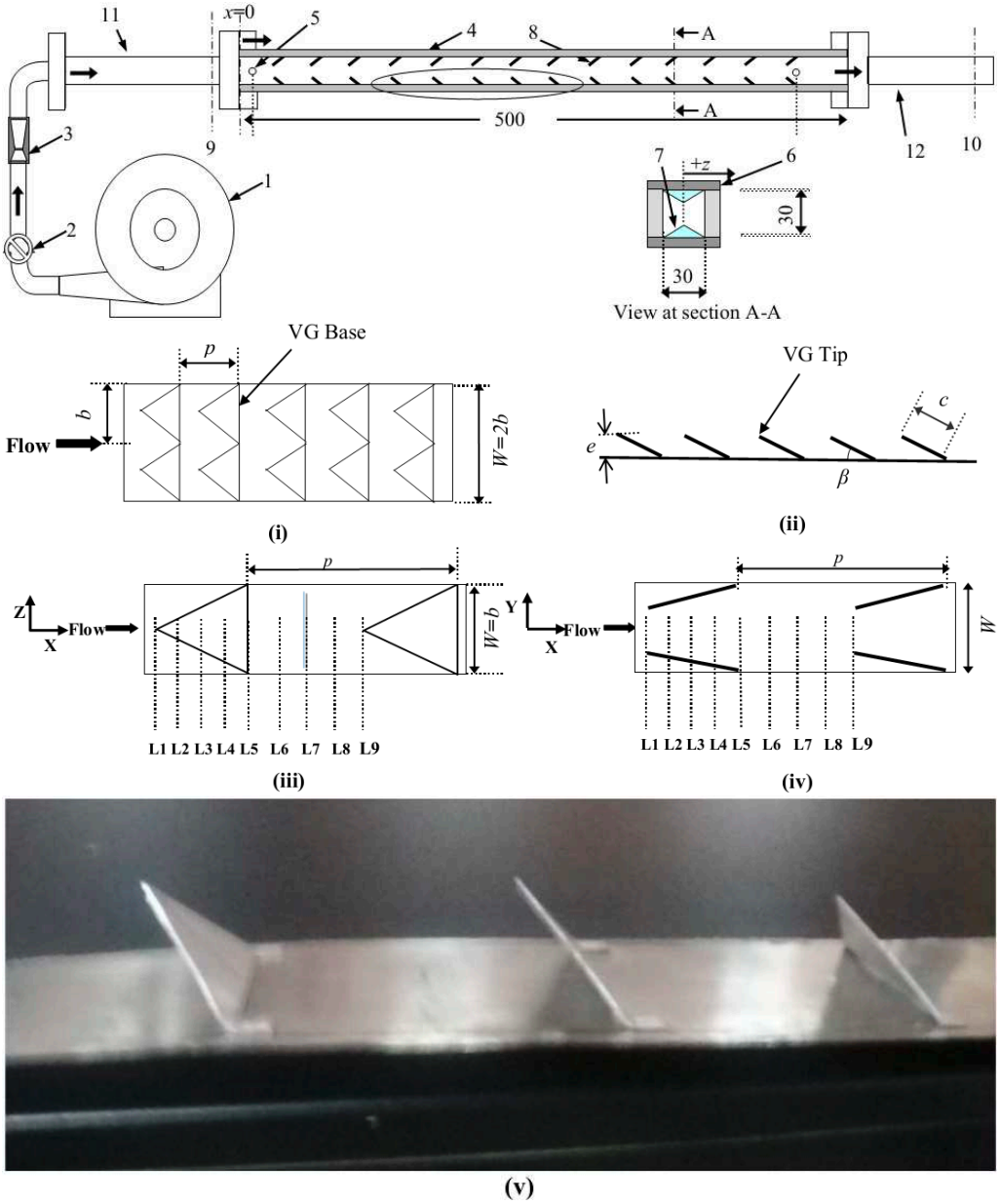

FIG. 1: (a) Schematic diagram of experimental set-up; (b) geometrical parameters of delta wing VGs; (i) top view for rough wall N = 2, (ii) side view for rough wall N = 2, (iii) top view for rough wall N = 1, (iv) top view for smooth wall N = 1, and (v) photograph showing the stainless steel foil with the VGs mounted on it

test section. A valve downstream of the blower controlled the flow through the test section. The test section consisted of two sides made of 0.1 mm thick stainless steel (SS) foil and two sides made of 10 mm thick Perspex to get a 500 mm long duct with a 30 mm $\times$ 30 mm square cross

section. The thickness of the SS foil was measured randomly at several locations; the maximum deviation from the nominal value was less than 0.001 mm. The variation in cross section due to this change was computed to be negligible and therefore ignored, since the side walls made of Perspex were accurately machined to the required dimensions. The maximum variation in the heat flux was therefore equal to 1%, and this was assumed to be the uncertainty in heat flux in calculating the uncertainty in the Nusselt number. The aluminum delta wings were cut such that two small 2 mm $\times$ 2 mm square cross-section appendages were glued to the foil (or Perspex) with RTV silicone. Therefore, the thermal contact resistance between the fin and the surface could be assumed to be high.

A fin analysis by Nalawade (2007) showed that even if the thermal contact is perfect, the fin effect can be ignored. Copper bars soldered to the SS foil at the inlet and exit sections were connected to a low voltage high current DC power source to heat the steel foil. The foil was painted black on the outside using matt finish blackboard paint to obtain as high an emissivity as possible to permit temperature measurement using an infrared camera. The inner side exposed to the flowing fluid was kept shiny to keep radiation losses to a minimum. The entire test section except the heated walls was insulated with a thick layer of ceramic wool. Delta wing type VGs were cut from a 0.4 mm thick aluminum sheet to the required size, bent to obtain the required height, and glued to the wall at the required spacing to form the rough walls. The top view and side view of the circled section in Fig. 1(a) are shown in Figs. 1(b) (i) and 1(b) (ii), where the various geometrical parameters of the delta wing VGs when a single or two VGs are located at each given axial location are shown. The height of the VG 'e' is the normal distance between the base surface and the tip, 'p' is the pitch between two successive VGs, 'b' is length of the base of the VG, and D_h is the hydraulic diameter of the duct. A photograph of the SS foil with the VGs mounted on it is shown in Fig. 1(b) (v). The local heat transfer coefficients are plotted at a few streamwise locations between two VGs in section 3. L1 and L9 represent the axial location of the tip of two successive VGs, and L5 corresponds to the base of the first of the two VGs as shown in Fig. 1(b) (iii). The divisions L1 to L5 are equidistant and represent the region on the wall beneath the VG while the divisions between L5 and L9 are also equally spaced between the base of VG and tip of the subsequent VG. The nondimensional parameters Re, p/e, e/D_h, D_h/b (or N) and Λ that are varied in this study are shown in Table 1.

An infrared camera (Micron Microspec 4) was used to measure the steady state temperature of the blackened outer surface of the SS foil. The small thickness of SS foil ensures negligible lateral conduction, enabling measurement of the local variations in heat transfer. The calculated temperature difference between the outer and inner walls was ignored since the calculated value using a 1D heat conduction model with volumetric heat generation equal to the maximum value utilized in the experiment was less than 0.01°C, which is well within the limits of experimental uncertainty of the present measurements.

An upstream unheated length of the test duct ($L/D_h = 16.5$) was provided to establish a hydrodynamically fully developed flow. The bulk fluid temperatures at the inlet and outlet of the test section, T_{in} and T_{out}, were measured by using four pre-calibrated Chromel-Alumel thermocouples ('K' type); the inlet temperature measurement locations were about one hydraulic diameter upstream of the start of the heated section. A proper mixed mean temperature at the outlet was obtained by measuring the temperatures after making the fluid exiting the test section to flow through an insulated section which was ten hydraulic diameters long and contained mixing devices.

A pre-calibrated digital voltmeter and ammeter of the proper range and resolution (with least counts equal to 0.01 V and 0.01 Amp, respectively) were used to measure the voltage drop

TABLE 1: Variation of Parameters in Present Study

N	e/D_h	p/e	Λ	Re $\times$ 10^{-3}
1	0.1	8, 12, 16	1.66	8, 12, 16, 20, 24
		8, 12	2.50	
		6, 8, 12	4.00	
		4, 6, 8, 10, 12	6.93	
		4, 6, 8, 12	14.93	
	0.15	2, 4, 6	6.93	
		10, 20	6.67	
	0.2	6, 8, 12, 16	1.66	
		6	2.50	
		6	4.00	
		2, 4, 6	6.93	
	0.3	3, 4, 6, 8, 12, 16	1.66	
		3, 6	2.50	
		3, 4, 6	4.00	
	0.4	3, 4, 6, 12	1.66	
	0.5	1.6, 2.4, 3.2	1.66	
		2.4	2.5	
		2.4	4.00	
2	0.1	12, 16	1.66	
		4	2.50	
		4, 6, 8	4.00	
		4	6.93	

(V) across and current (I) through the steel foil to calculate the electrical power supplied. The heat loss from the heated wall to the surrounding ambient was experimentally determined by filling the square channel with an insulating material, giving a small power input to the heater, and measuring the wall temperature at steady state. The exercise was repeated for several other values of heat input to obtain an equation relating the heat loss (Q_{loss}) to the difference between ambient and wall temperature, which was used to compute the heat loss for a given surface temperature. The difference between electrical energy supplied ($Q_{elec} = VI$) and the heat loss (Q_{loss}) gave the actual heat supplied to the system (Q_{sup}), as shown in Eq. (1).

$$Q_{sup} = Q_{elec} - Q_{loss} \tag{1}$$

The difference between the heat supplied to the system (Q_{sup}) and the enthalpy rise of air from inlet to exit of the test duct [$Q_{fluid} = \dot{m} c_p (T_{out} - T_{in})$] was always less than 10%, which was within the limits of experimental uncertainty and therefore considered acceptable. The bulk temperature difference between the inlet and outlet sections varied between 3°C and 10°C, and the electrical power input varied between 60W and 100W. The maximum energy imbalance was observed for smaller power inputs due to higher uncertainties in measured temperature values. Such experiments were repeated to confirm reproducibility of the data.

The pressure drop was measured at ambient conditions (i.e., without heating the test duct) using a differential manometer, and the friction factor was determined using Eq. (2).

$$f = \frac{\Delta p}{(4L/D_h)\left(\rho \overline{V}^2/2\right)} \tag{2}$$

$$\mathrm{Nu}_L(x,y,z) = \frac{D_h\left[VI/A - Q_{loss}/A\right]}{k\left[T_w(x,y,z) - T_b(x)\right]} \tag{3a}$$

$$\begin{aligned} \mathrm{Nu}_{sa,r}(x) &= \left[\int_{y=-0.5D_h}^{y=0.5D_h} \mathrm{Nu}(x,y,z=\pm 0.5D_h)dy\right]/D_h \\ \mathrm{Nu}_{sa,s}(x) &= \left[\int_{z=-0.5D_h}^{z=0.5D_h} \mathrm{Nu}(x,y=\pm 0.5D_h,z)dz\right]/D_h \end{aligned} \tag{3b}$$

$$\mathrm{Nu}_{ss} = \frac{\int_{x=0}^{x=L} \mathrm{Nu}_{sa,s}(x)dx}{L}, \qquad \mathrm{Nu}_{rr} = \frac{\int_{x=0}^{x=L} \mathrm{Nu}_{sa,r}(x)dx}{L} \tag{3c}$$

$$T_b(x) = T_b(x=0) + \frac{(1-x/L)Q_{sup}}{\dot{m}c_P} \tag{3d}$$

The temperature distribution of the heated walls [$T_w(x,y,z)$] was used to calculate the local Nusselt number [$\mathrm{Nu}_L(x,y,z)$], as shown in Eq. (3a). This was then used to find the spanwise average Nusselt number at each axial location [$\mathrm{Nu}_{sa,s}(x)$] and [$\mathrm{Nu}_{sa,r}(x)$] for the rough and smooth walls, respectively, as shown in Eq. (3b). The overall wall averaged Nusselt number for smooth and rough walls (Nu_{ss} and Nu_{rr}, respectively) were calculated as shown in Eq. (3c). The bulk temperature $T_b(x)$ at any given streamwise location, x, was calculated from Eq. (3d).

The friction factor (f) for the rough channel of the present study is normalized by that for fully developed turbulent flow in smooth circular tubes, (f_s), which is calculated by Eq. (4) at constant Re.

$$f_s = 0.316\mathrm{Re}^{-0.25} \tag{4}$$

The effective Reynolds number (Rec) for a smooth section which will correspond to the same pumping power required to maintain a given Re in the channel with VGs present is obtained by using Eq. (5).

$$f \times \mathrm{Re}^3 = 0.316 \times (Rec)^{2.75} \tag{5}$$

The Gnielinski (1976) correlation for fully developed flow in smooth circular tubes was used to compute the Nusselt numbers, Nu_s and Nu_c at Re and Rec, respectively. The Nusselt number ratio $\mathrm{Nu}_{rr}/\mathrm{Nu}_s$ gives the heat transfer augmentation for constant flow rate. The $\mathrm{Nu}_{rr}/\mathrm{Nu}_c$ is the ratio of heat transfer conductance at constant pumping power and equal area and is identical to $(\mathrm{St}/\mathrm{St}_s)\,/\,(f/f_s)^{1/3}$ reported by Webb and Eckert (1972) for these conditions, and is often referred to as the Thermal Performance Parameter (TPP). The value of this parameter must be greater than unity for the enhancement methodology to be acceptable.

The thermocouples were calibrated to obtain an uncertainty less than 0.5°C with a 99.7% confidence interval. The thermal camera was calibrated by using a nearly isothermal copper block, whose temperature was measured by three thermocouples embedded in it. An SS foil,

painted black, identical to that used in the test section, was soldered to the copper block. The copper block was heated by an electrical heater attached to it, and the temperature of the foil was measured by the thermal camera. The calibration curve was generated by heating the copper block with different power levels and measuring the temperature by the thermal camera along with the thermocouples. The corresponding uncertainty was evaluated to be 1°C with a 99.7% confidence interval. The uncertainty in the pressure drop readings measured using a manometer was taken to be equal to 1 mm of water column. The corresponding uncertainties for mass flow rate, pressure drop, friction factor, and Nusselt number were calculated to be 6.1%, 9.0%, 11.3%, and 10%, respectively.

3. RESULTS AND DISCUSSION

Initial measurements were made using the channel with smooth walls, and the data compared with well-known correlations for friction [Eq. (4)] and heat transfer (Gnielinski, 1976). The deviations shown in Fig. 2 are within 10% for the friction factor and 5% for the heat transfer, which are within the limits of uncertainty presented earlier. The parameters involved in the study are large, and only representative results for Nusselt number and friction factor are presented here. Complete details are presented by Nalawade (2007). However, the entire data set was used to develop the final correlations.

3.1 Effect of Number of Walls Where VGs are Located

The delta wing VGs can be placed on one, two, or on all four walls in a channel. Variations of geometric parameters were chosen arbitrarily. The effect on the channel average Nusselt number ratios and friction factor ratios for these three different cases for one choice of geometric parameters are shown in Fig. 3.

The heat transfer coefficient ratio and friction factor ratio increase as the number of roughened walls increase. The magnitudes are highest for the four-wall case as expected. The VGs on a single roughened wall create an overall mixing of the flow affecting the shear at the adjacent walls, as well as the opposite wall. The friction factor for the roughened four walls is more than four times the single wall roughened single wall, indicating significant interaction of the flow between the opposite/adjacent walls. The Nusselt number at constant pumping power for the two-wall roughened case is only marginally different from the four-wall case, whereas

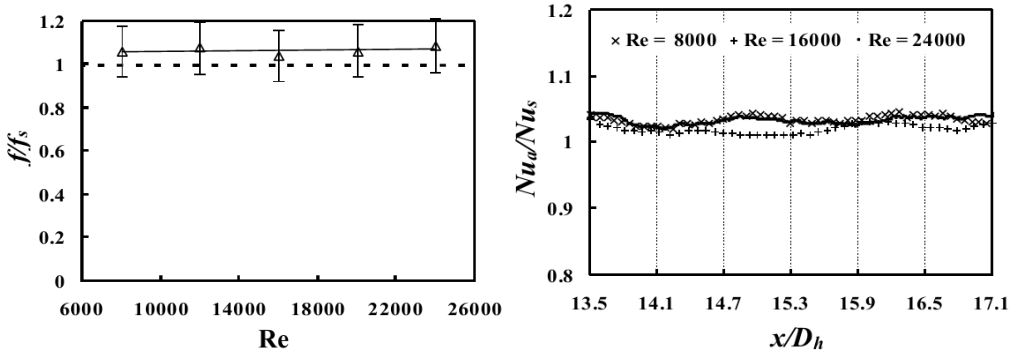

FIG. 2: Comparison of smooth wall friction and heat transfer characteristics

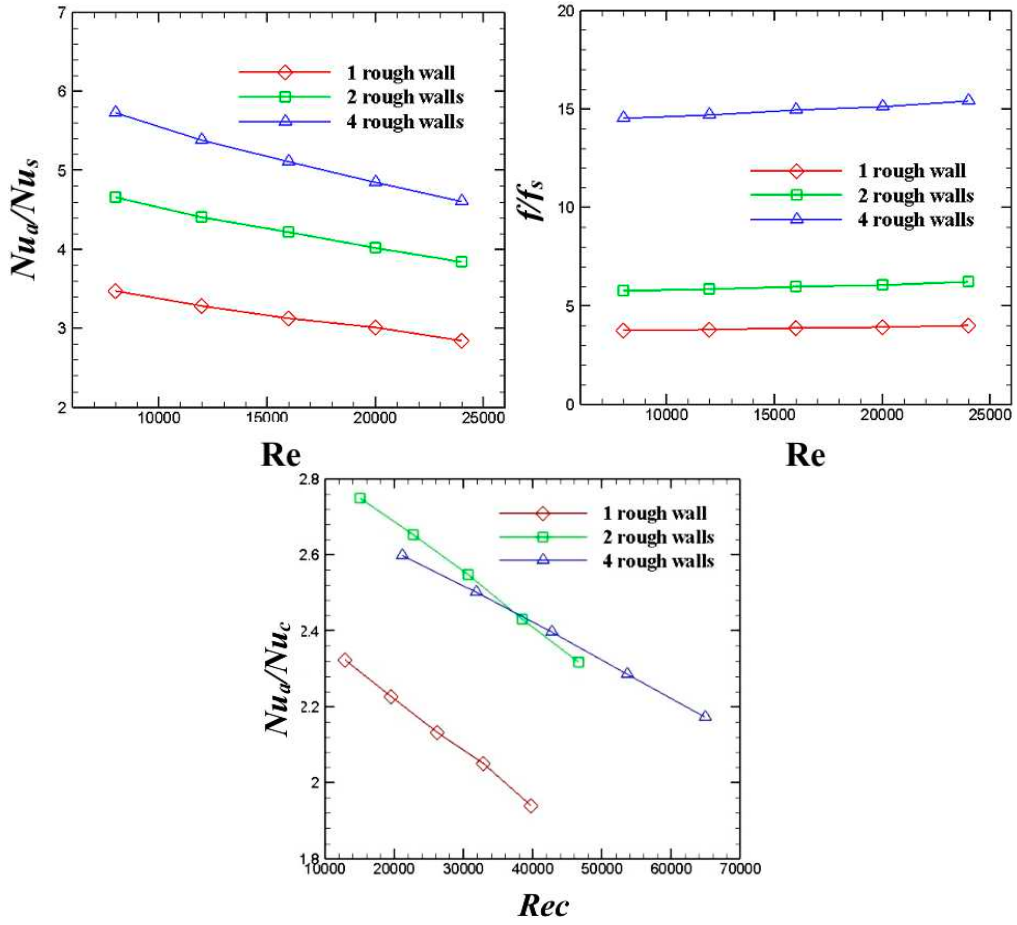

FIG. 3: Comparison of channel average performance ($\mathrm{Nu}_a/\mathrm{Nu}_s$, f/f_s and $\mathrm{Nu}_a/\mathrm{Nu}_c$) between one, two, and four walls roughened with VGs, ($\Lambda = 6.9$, $p/e = 6$, $e/D_h = 0.1$)

the pressure drop penalty is significantly lower. This example was therefore used in a detailed parametric study.

The difference in the Nusselt number values on the smooth and the VG roughened wall was then investigated. The Nusselt number enhancement for $e/D_h = 0.1$ is shown in Fig. 4 for a selected set of parameters. The Nusselt number values for smooth walls are only about 10% lower than those for the rough walls, and therefore results are reported predominantly for the rough wall in the present work. The details of smooth wall data are described by Nalawade (2007).

3.2 Local Heat Transfer on Smooth and Roughened Walls

The local heat transfer enhancement for the rough wall with $\Lambda = 4$, $e/D_h = 0.1$, and $p/e = 8$ for Re = 16,000 for selected stream-wise locations is shown in Fig. 5(a). L2 to L5 and L6 to L9 represent locations upstream and downstream of the VG as shown in Figs. 1(b) (iii) and 1(b) (iv), respectively. The VG pushes the cooler mainstream fluid towards the wall causing

higher heat transfer coefficients just underneath the VG. The fluid tends to curl around the VG forming vortex structures from each edge that move in the downstream direction, resulting in enhanced heat transfer coefficients. The vortex structures do not interact strongly with each other, giving rise to higher mixing in the edge regions compared to the central region and resulting in higher heat transfer coefficients in the edge regions for all locations L6 to L9. The local data for an increased $\Lambda = 6.9$, $e/D_h = 0.1$, and $p/e = 8$ for Re = 16,000 is shown in Fig. 5(b). An increase in the aspect ratio of VG results in an increased angle of attack, making it easier for the mainstream fluid to be pushed towards the wall and resulting in highest heat transfer coefficients along the VG centerline region. In the downstream region with increased angle of attack, the strength of the vortex structure from each edge increases which tends to make the mixing regions from each edge come closer to each other and the heat transfer over the entire region increases. A schematic of the possible flow path is shown in Fig. 6.

The corresponding smooth wall heat transfer coefficients are shown in Fig. 7. The smooth wall heat transfer coefficients are highest close to the roughened wall. The fluid directed by the

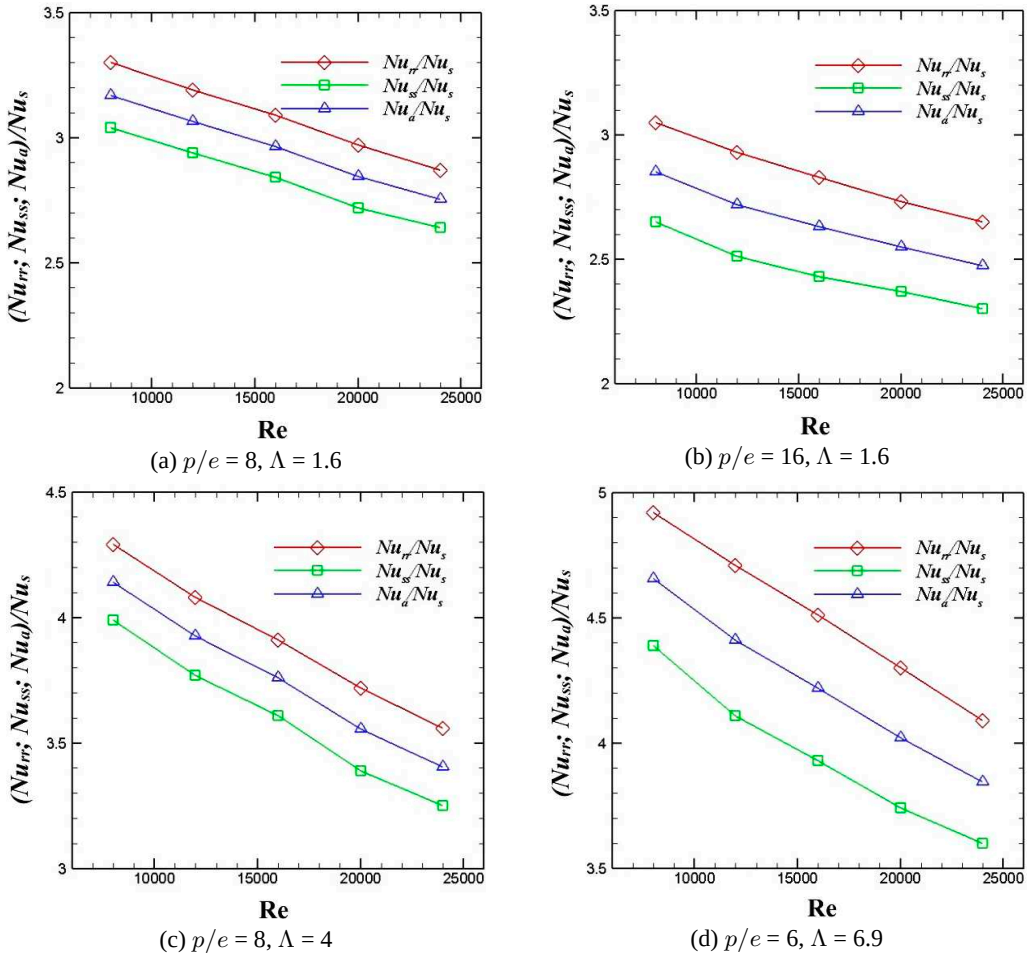

(a) p/e = 8, Λ = 1.6 (b) p/e = 16, Λ = 1.6

(c) p/e = 8, Λ = 4 (d) p/e = 6, Λ = 6.9

FIG. 4: Smooth wall, rough wall and channel average heat transfer enhancement performance with two opposite walls roughened with VGs, ($e/D_h = 0.1$)

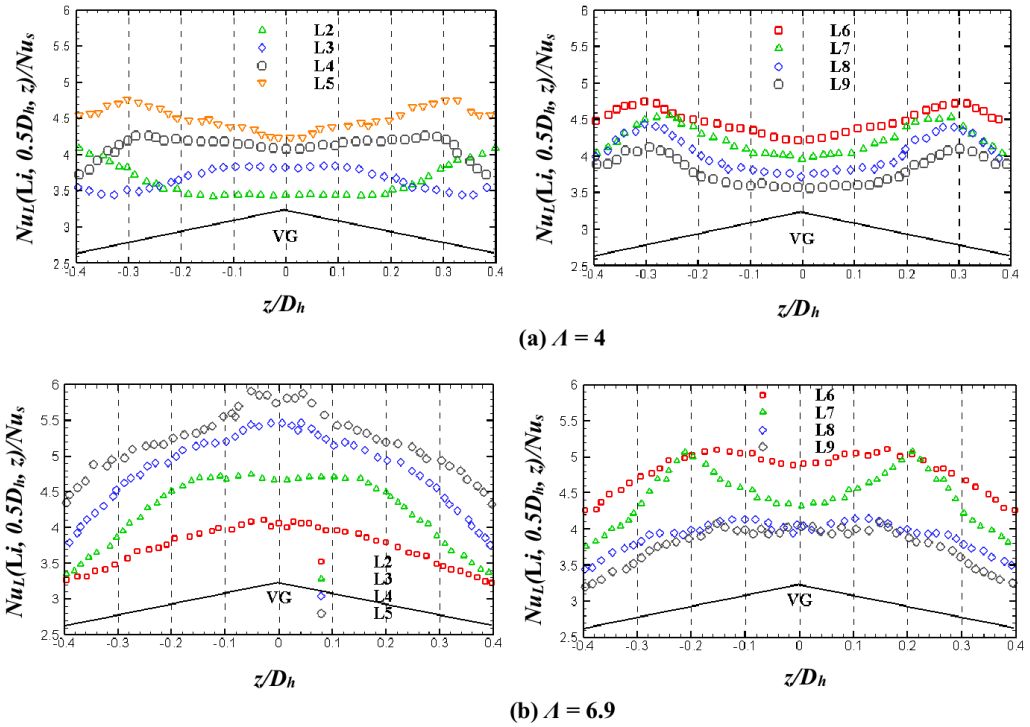

FIG. 5: Spanwise distribution of $\mathrm{Nu}_L/\mathrm{Nu}_s$ for the rough wall upstream and downstream of the VG for (a) $\Lambda = 4$ and (b) $\Lambda = 6.9$, ($p/e = 8$, $e/D_h = 0.1$, Re = 16,000)

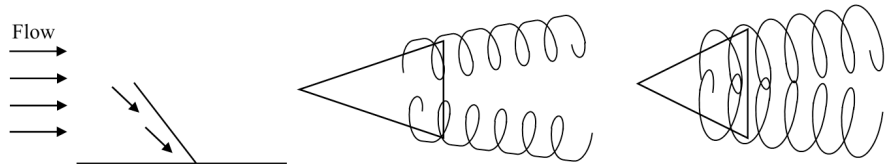

FIG. 6: Flow path around the VG

VG towards the base exits from underneath the VG in a transverse direction, and moves towards the smooth wall. The interaction of this flow with the smooth wall at $z/D_h = \pm 0.5$ results in enhanced heat transfer coefficients over the smooth wall. The cross flow weakens as it moves along the smooth wall towards its center (i.e., $y/D_h = 0$) causing a reduction in the heat transfer coefficients in the region $0 < y/D_h < 0.5$. The cross flow from the VG on the opposite wall results in a similar behavior in the region $-0.5 < y/D_h < 0$. Representative contour plots shown in Fig. 8 depict the behavior discussed above.

The distribution of local Nusselt number ratio on the roughened wall for ($p/e = 8$, $e/D_h = 0.1$, $\Lambda = 4$) for the case with two VGs at an axial location (N = 2) is shown in Fig. 9. A separate peak is seen for each of the two VGs at location L5, as the mainstream fluid is directed to the region underneath each VG. Similarly, the four vortex structure in the downstream region results

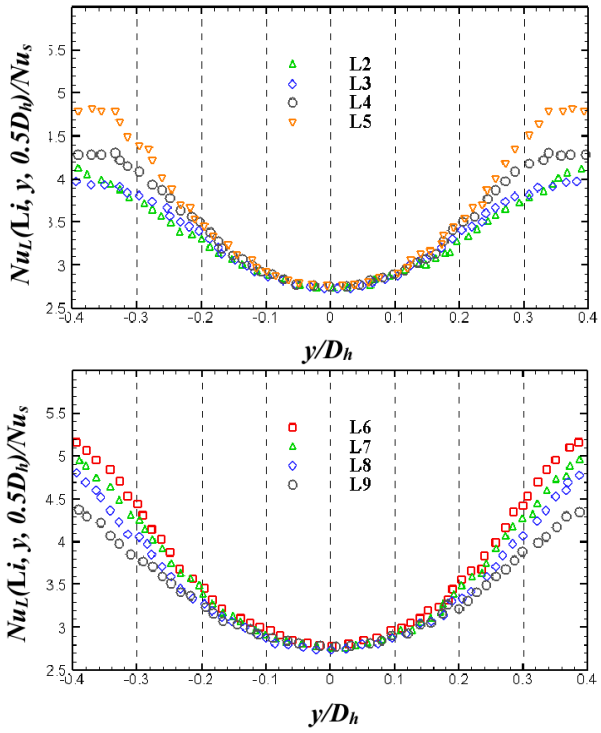

FIG. 7: Spanwise distribution of $\mathrm{Nu}_L/\mathrm{Nu}_s$ for the smooth wall upstream and downstream of the VG, ($p/e = 8$, e/D_h = 0.1, $\Lambda = 4$, Re = 16,000)

in two peaks in the downstream region. The heat transfer coefficients gradually decay as the flow moves from L5 to L8 due to viscous forces.

The penetration of the mainstream fluid underneath the VG is larger for the N = 2 case when compared to N = 1 since for the same aspect ratio the angle of attack increases, resulting in high values of heat transfer coefficient in the base region with a central peak. Two vortex structures would emerge from each VG, resulting in a better mixing in the downstream region for this case.

3.3 Span-Wise Averaged Data

The vortex generators aid in rapid mixing of the flow. Local data after the first few vortex generator elements indicated a nearly constant average heat transfer coefficient over the span of a vortex generator. The flow can therefore be considered to be thermally fully developed, and data only pertaining to this region are presented.

3.3.1 Effect of Pitch-to-Height Ratio and Height-to-Hydraulic Diameter Ratio (N = 1)

The variation of the spanwise averaged heat transfer along the axial direction for rough and smooth walls for $e/D_h = 0.1$ and 0.2 is shown in Fig. 10. The smaller e/D_h gives smaller fluctuations in the axial direction because the p/e ratio is the same for the two cases. The rise in the heat transfer coefficients starts approximately where the VG starts and increases monotonically till the base of the VG due to the mainstream fluid being pushed towards the base. The slope of

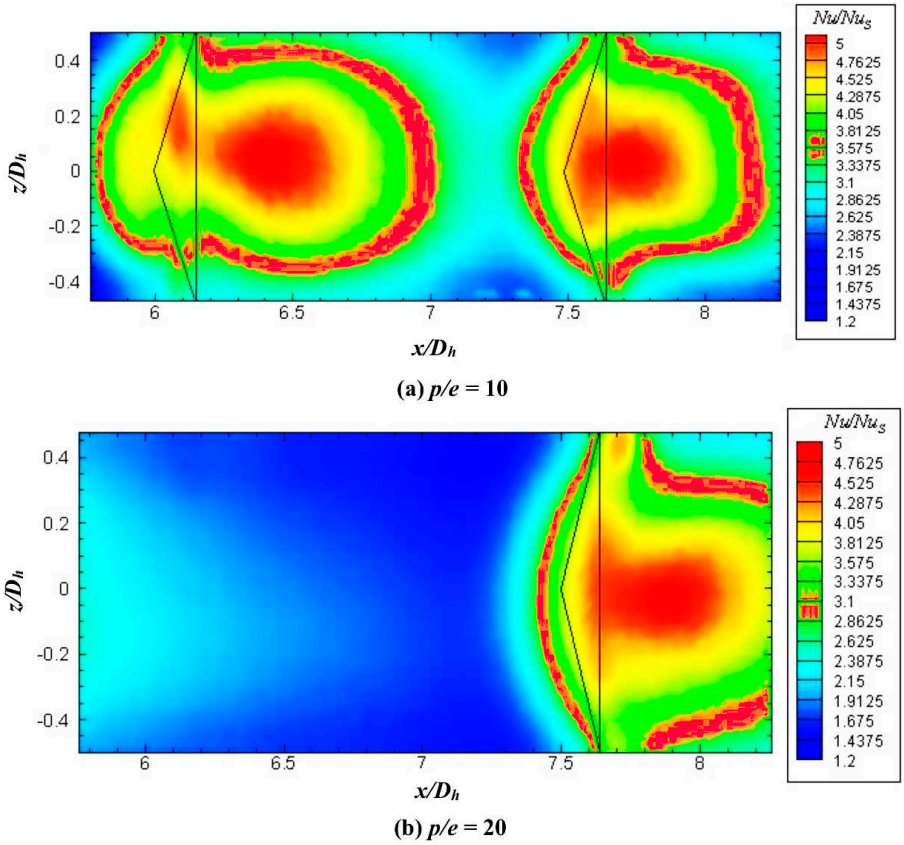

FIG. 8: Local distribution of Nu/Nu$_s$ for the rough wall ($y = 0.5D_h$) for (a) $p/e = 10$ and (b) $p/e = 20$, ($e/D_h = 0.15$, $\Lambda = 6.67$, Re = 20,000)

the rise therefore is larger for the larger e/D_h case since the same aspect ratio is maintained. The vortex structure dissipates until the next VG is encountered and therefore the ratio of the peak to valley heat transfer is larger for the $e/D_h = 0.2$ case. The enhancement in heat transfer in the downstream direction is large due to the vortex structure downstream of the VG, which then decreases as the mixing zone gets dissipated along the axial direction due to viscous effects. The smooth wall heat transfer is enhanced due to the cross flow generated as the fluid exits from beneath the VG. The strength of this crossflow is mitigated very close to the base where the resistance for fluid exiting from underneath the VG increases due to friction in the narrow gap between the VG and wall on which it is mounted, possibly accounting for the shift of the peak heat transfer location slightly upstream of the base of the VG for small e/D_h values.

3.3.2 Effect of Aspect Ratio

The effect of Λ on the variation of spanwise averaged heat transfer along the axial direction is shown in Fig. 11. The angle of attack is noticed to increase with Λ ($\beta = 7.18°$, 11.53°, and 20.27°, for $\Lambda = 2.5$, 4, and 6.9, respectively) since the e/D_h remains constant. The spanwise averaged Nusselt number peak increases with increase in Λ due to the increase in angle of attack.

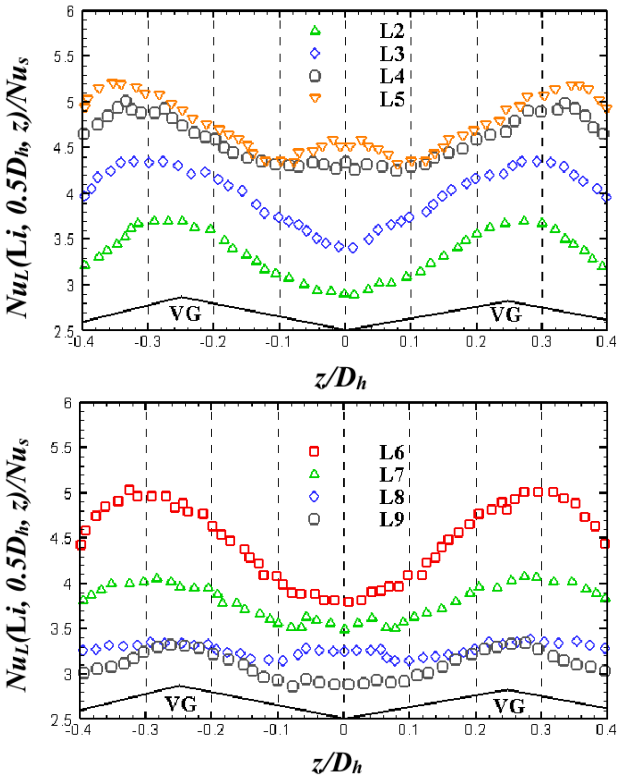

FIG. 9: Spanwise distribution of $\mathrm{Nu}_L/\mathrm{Nu}_s$ for the rough wall upstream and downstream of the VG, ($p/e = 8$, $e/D_h = 0.1$, $\Lambda = 4$, N = 2, Re = 16,000)

The distance over which the mixing zone created by the longitudinal vortex structure can dissipate in the downstream direction is constant, since the p/e is constant. The lowest heat transfer coefficients in between the VGs are therefore higher for the larger Λ values. The difference in between the highest and lowest heat transfer coefficient values increases with increase in the value of Λ and the overall average is found to be higher for $\Lambda = 6.9$.

3.3.3 Spanwise Two VG Rows

The VGs reduce in size with increasing N and the physical dimensions of the experimental setup used in the present investigation prevented use of more than two VGs at a given axial location. The spanwise averaged Nusselt number augmentation for constant Reynolds number, Λ, p/e, and e/D_h for the N = 1 and N = 2 cases is shown in Fig. 12. It is observed that the local peak of heat transfer is higher for the N = 2 case since the angle of attack is higher. The dissipation is also more rapid since the vortex structure is stronger in addition to the influence of interaction between the mixing regions created downstream of each VG. The peak to valley heat transfer coefficient is therefore larger for the N = 2 case even though the other non-dimensional parameters are maintained equal.

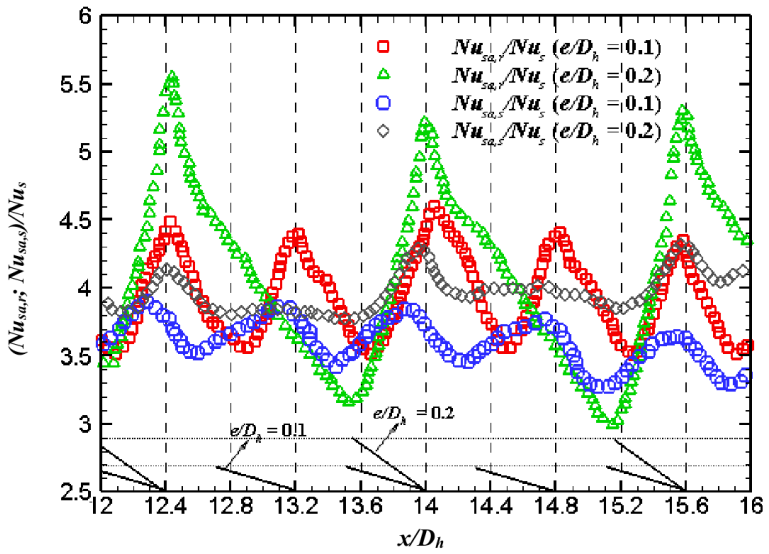

FIG. 10: Comparison of spanwise averaged axial distribution of nusselt number for smooth (Nu_{sa}, s/Nu_s) and rough walls (Nu_{sa}, r/Nu_s) for $e/D_h = 0.1$ and 0.2, ($p/e = 8$, $\Lambda = 4$, Re = 16,000)

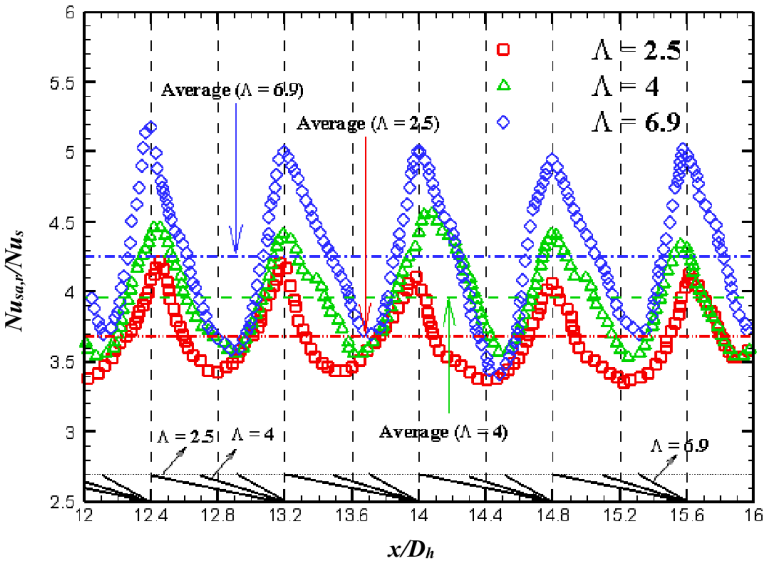

FIG. 11: Comparison of spanwise averaged axial distribution of Nu_{sa}, r/Nu_s for different Λ, ($p/e = 8$, $e/D_h = 0.1$, Re = 16,000)

3.4 Overall Averaged Data

3.4.1 Effect of Pitch-to-Height Ratio and Height-to-Hydraulic Diameter Ratio (N = 1)

The overall averaged heat transfer behavior and pressure loss as a function of p/e for $\Lambda = 1.6$ for $e/D_h = 0.1$ and 0.5 are shown in Figs. 13(a) and 13(b), respectively. The $\mathrm{Nu}_{rr}/\mathrm{Nu}_s$ ratios

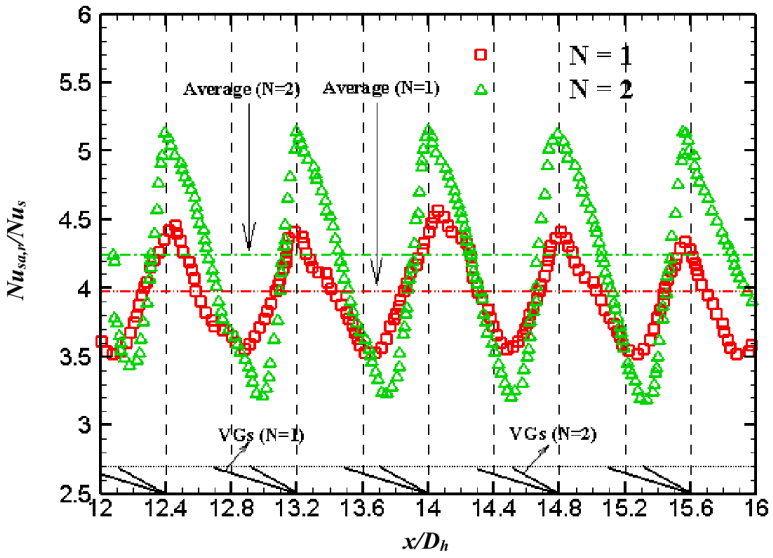

FIG. 12: Comparison of spanwise averaged axial distribution of Nu_{sa}, r/Nu_s for N = 1 and 2, ($p/e = 8$, $e/D_h = 0.1$, $\Lambda = 4$, Re = 16,000)

increase when p/e ratio is reduced initially, but then they level off with further reduction in p/e. The heat transfer values between successive VGs are expected to rise with reducing p/e ratio since the flow downstream of one VG encounters the next VG before the mixing region dissipates completely. However, further reduction in spacing brings the VGs closer to one another, which impedes the penetration of the fresh mainstream fluid towards the wall and the heat transfer coefficients level off. A further reduction in p/e would cause the heat transfer coefficient to reduce further. An optimum pitch-to-height ratio therefore exists for obtaining maximum heat transfer coefficient values when other parameters are kept constant.

An increase in e/D_h results in an increased projected area that causes increased mixing and therefore increased Nusselt number values and also a higher pressure drop. The maximum enhancement in heat transfer coefficient is noticed for the $e/D_h = 0.5$ case, but the pressure drop increase is also considerable. The maximum enhancement based on constant pumping power is obtained for the $e/D_h = 0.1$ case, amongst the cases of e/D_h studied.

The smallest pitch-to-height ratios used in the current investigation were limited by fouling between successive VGs for the $e/D_h = 0.1$ case, and limitations of accurately positioning the adjacent VGs for the $e/D_h = 0.5$ case. The highest e/D_h value used in the entire experimental program was equal to 0.5 since larger values were not possible for an in-line configuration. In the present investigation, the maximum enhancement in heat transfer coefficient was noticed to occur at a p/e spacing corresponding to the one where the tip of one VG was approximately at the same axial location as the base of the preceding VG.

3.4.2 Effect of Aspect Ratio

The effect of variation in Λ (for $e/D_h = 0.1$ and $p/e = 8$) on the overall averaged values (i.e., $\mathrm{Nu}_{rr}/\mathrm{Nu}_s$, f/f_s, and $\mathrm{Nu}_{rr}/\mathrm{Nu}_c$) is shown in Fig. 14, where Λ = 6.9 is very close to the

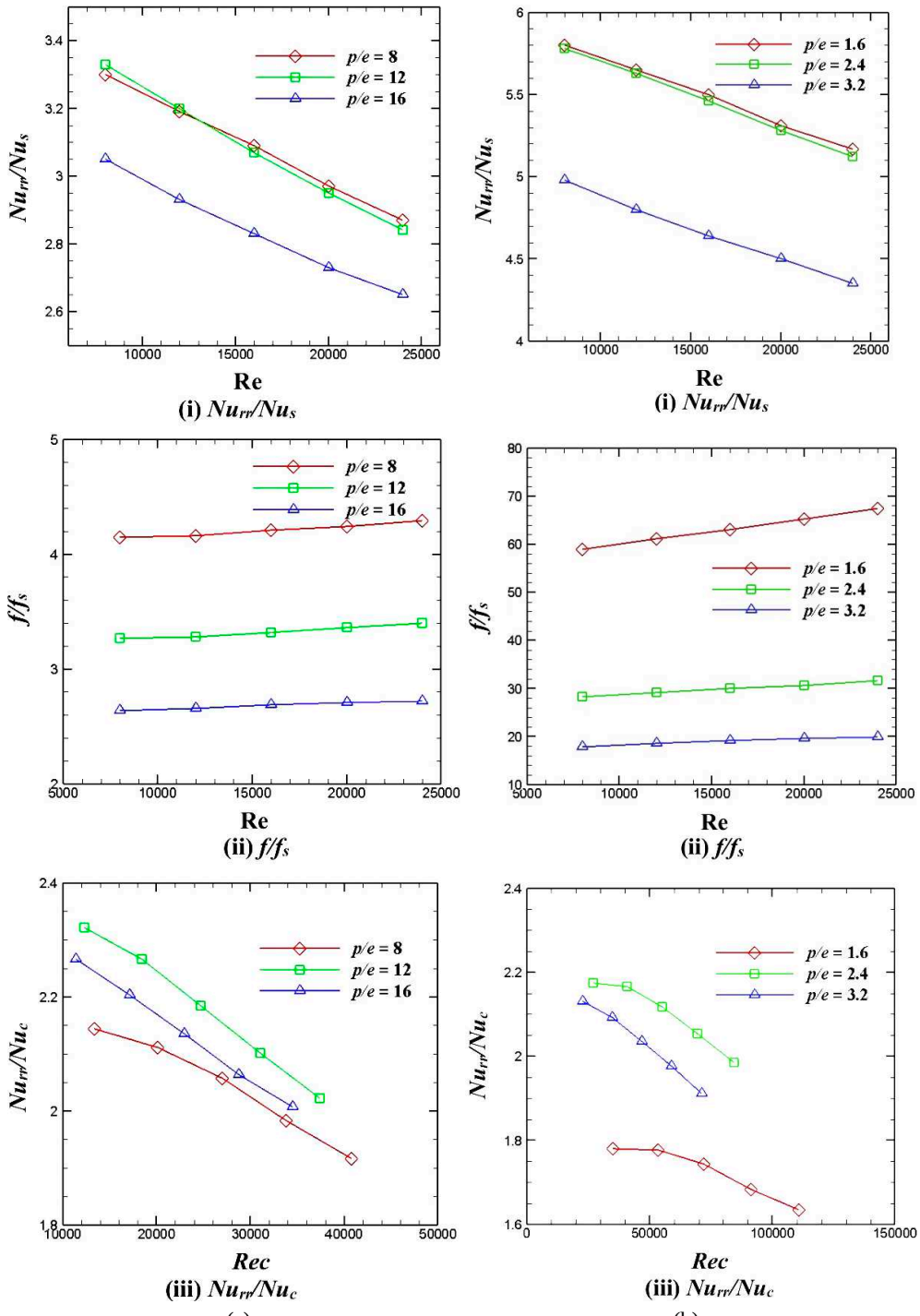

FIG. 13: (a) Variation in (i) $\mathrm{Nu}_{rr}/\mathrm{Nu}_s$, (ii) f/f_s, (iii) $\mathrm{Nu}_{rr}/\mathrm{Nu}_c$ with p/e, ($\Lambda = 1.6$, $e/D_h = 0.1$); (b) Variation in (i) $\mathrm{Nu}_{rr}/\mathrm{Nu}_s$, (ii) f/f_s, (iii) $\mathrm{Nu}_{rr}/\mathrm{Nu}_c$ with p/e, ($\Lambda = 1.6$, $e/D_h = 0.5$)

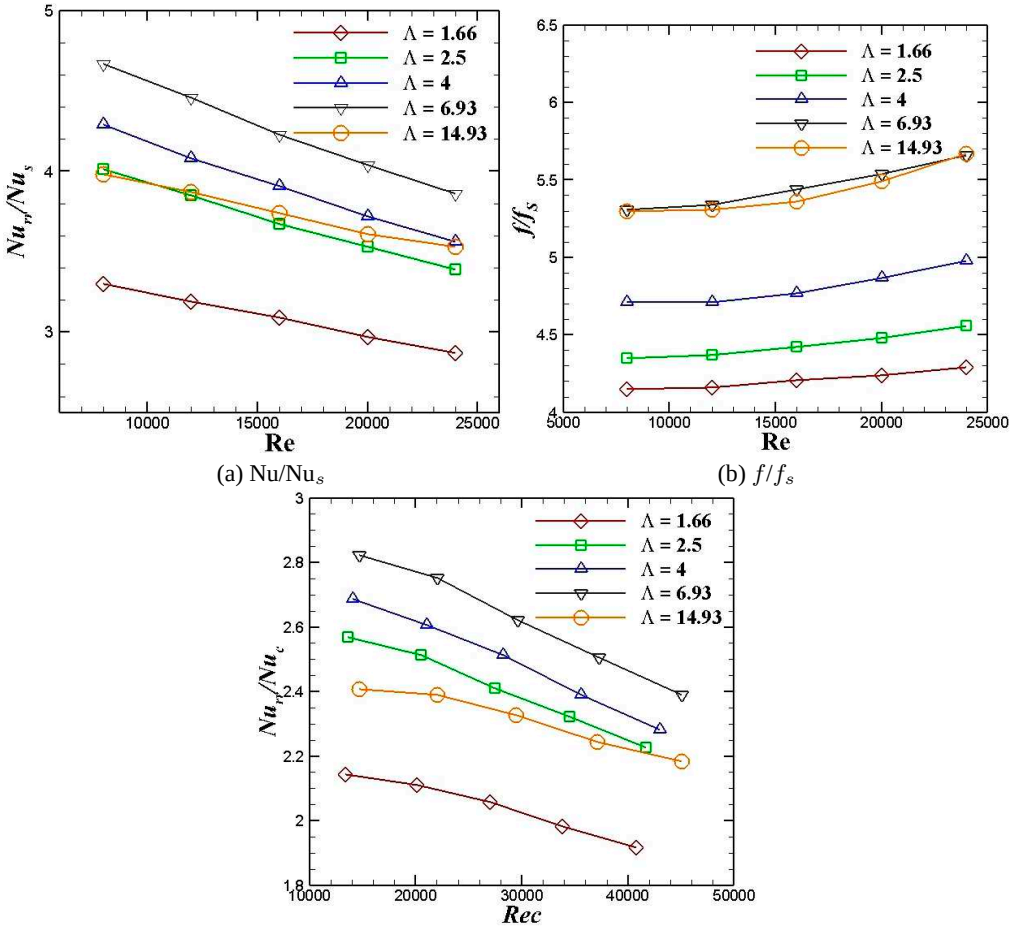

(a) Nu/Nu$_s$ (b) f/f_s

(c) Nu/Nu$_c$

FIG. 14: Variation in Nu$_{rr}$/Nu$_s$, f/f_s and Nu$_{rr}$/Nu$_c$ with Λ, ($p/e = 8$, $e/D_h = 0.1$)

optimal value. An increase in Λ results in increased Nusselt number values initially, but for very large values the angle of attack becomes very large and the heat transfer deteriorates due to the breakdown of the vortex structure in the downstream region. The breakdown of the vortex structure results in mixing but the mainstream fluid is no longer directed properly towards the wall, which results in lower heat transfer coefficients. However, the mixing fluid causes the pressure drop to increase, resulting in smaller heat transfer enhancement for constant pumping power. In addition, the diversion of the mainstream fluid towards the wall also reduces due to increased angles of attack, which reduces the heat transfer coefficient values underneath the VG also.

3.4.3 Two Spanwise VG Rows

The aspect ratio was varied for the N = 2 case, keeping $p/e = 4$ and $e/D_h = 0.1$ (Fig. 15). The e/D_h was kept equal to 0.1 because it gave the best constant pumping power performance for

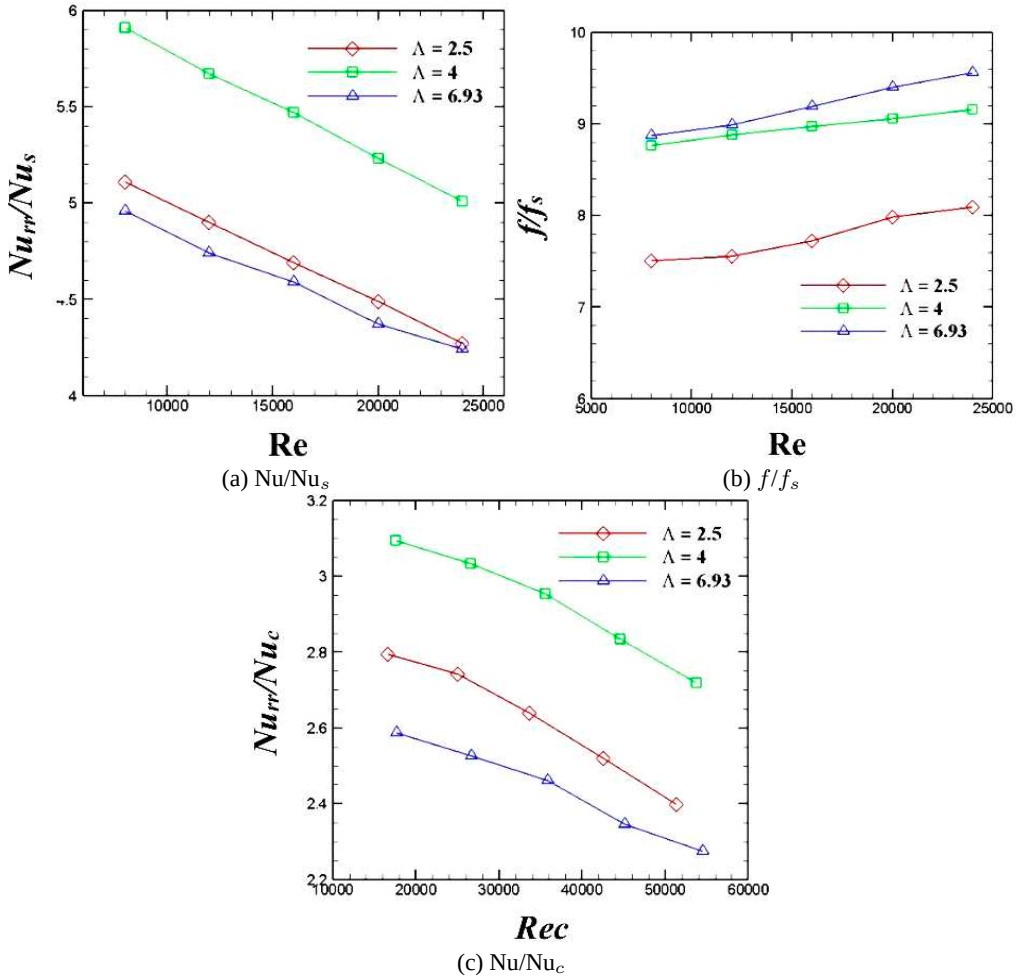

(a) Nu/Nu$_s$ (b) f/f_s

(c) Nu/Nu$_c$

FIG. 15: Variation in Nu$_{rr}$/Nu$_s$, f/f_s and Nu$_{rr}$/Nu$_c$ with Λ, (p/e = 4, e/D_h = 0.1, N = 2)

the N = 1 case. It can be observed that $\Lambda = 4$ is most suitable for N = 2. The pitch-to-height ratio (p/e) was varied, keeping the e/D_h and Λ constant (Fig. 16). It can be observed that $p/e = 4$ results in the best performance which again corresponds to the case where the base of one VG and the tip of the successive one are very close to each other.

The best performance with a single delta wing on the wall was obtained when $\Lambda = 6.9$, $e/D_h = 0.1$, and $p/e = 8$, where the highest enhancement ratio at the lowest Reynolds number (8000) was 4.7. The corresponding enhancement at constant pumping power ratio was observed to be 2.8 that reduced to 2.4 (as seen in Fig. 14) with increase in the Reynolds number to 25,000. Similar enhancements have been reported at constant Reynolds number values using similar delta wing vortex generators by Skullong et al. (2016). Singh and Ekkad (2017) reported values of the thermal hydraulic performance [defined as $(\mathrm{Nu}/\mathrm{Nu}_s)\,/\,(f/f_s)^{1/3}$] equal to about 2.0 at Reynolds number of 25,000. The above value (Nu$_{rr}$/Nu$_c$ = 2.4) when converted using their definition becomes about 2.0. However, for the two vortex generators at a spanwise location case,

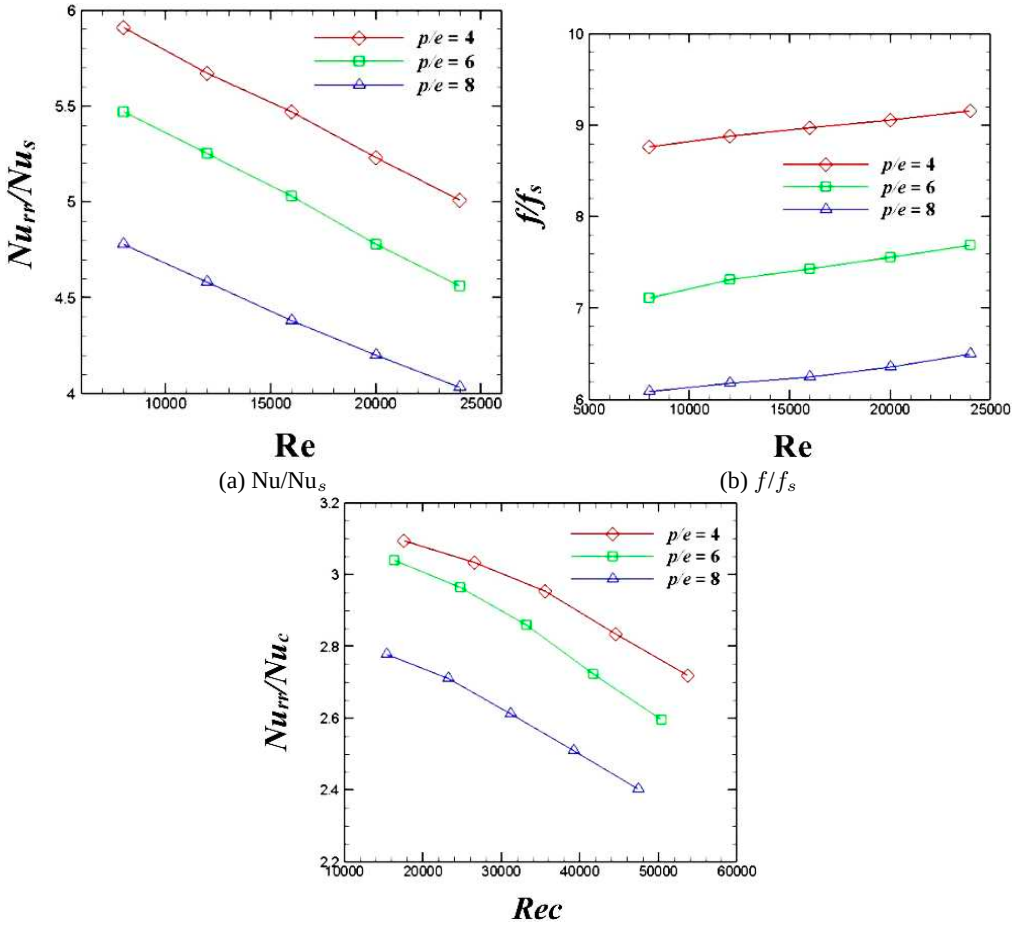

FIG. 16: Variation in $\mathrm{Nu}_{rr}/\mathrm{Nu}_s$, f/f_s and $\mathrm{Nu}_{rr}/\mathrm{Nu}_c$ with p/e, (Λ = 4, e/D_h = 0.1, N = 2)

the largest value of thermal hydraulic performance using their definition is obtained to be 2.8 for $\Lambda = 4$, $e/D_h = 0.1$, Re $= 8000$, and $p/e = 4$ [equal to 3.1 using present definition as shown in Fig. 15(c)]. The present configuration is therefore competitive with the high performance enhancement devices that have been reported.

3.5 Heat Transfer and Friction Factor Correlations

The number of parameters that influence the heat transfer performance is very large and therefore a correlation to predict the performance of a given VG geometry is desirable. A simple multi-variable regression analysis was attempted but the results were not satisfactory. Semi-empirical correlations were therefore developed on the basis of the law of the wall similarity analysis for rough surfaces reported by Han et al. (1984, 1988). In the present study, measurements were made in a square channel with two opposite walls roughened with VGs.

The friction roughness function for the present study can be assumed to be

$$R(e^+) = (f_r/2)^{-1/2} + 2.5\ln(2e/D_h) + 2.5 \tag{6}$$

$$\text{where} \quad e^+ = (e/D_h)\,\text{Re}\,(f_r/2)^{1/2}, \quad f_r = 2f - f_s; \quad \text{and} \quad f_s = 0.046\text{Re}^{-0.2} \tag{7}$$

Equation (6) is used to compute $R(e^+)$ for the various parameters of the present study. The average friction factor (f) is assumed as the arithmetic mean between the four-sided smooth channel (f_s) and the four-sided rough channel (f_r) friction factors.

The dependence of $R(e^+)$ on p/e, e/D_h, β, N, and e^+ of the present friction data (280 data points) obtained by using the law of the wall similarity analysis and multi-dimensional regression analysis can be represented as:

$$R\left(e^+\right) = \left\{\left[1.2633\,(p/e)^{0.44572}\,(\beta)^{0.19665}\left(e^+\right)^{0.058951}\right] / \left[(N)^{0.43314}\,(\Lambda)^{0.36258}\right]\right\} \tag{8a}$$

It is observed that the influence of the roughness Reynolds number (e^+) on $R(e^+)$ in Eq. (8a) is very small and therefore, neglecting its influence, the above equation [Eq. (8a)] can be written as shown below in Eq. (8b).

$$R\left(e^+\right) = \left\{\left[1.2633\,(p/e)^{0.41418}\,(\beta)^{0.26217}\right] / \left[(N)^{0.49321}\,(\Lambda)^{0.42692}\right]\right\} \tag{8b}$$

The deviation of Eq. (8b) is ± 15% for 96% of the data.

Similarly, the heat transfer roughness function $G(e^+)$ of the present study can be evaluated from Eq. (9).

$$G\left(e^+\right) = \left\{(f_r/2)^{1/2}\,(1/\text{St}_{2r}) + 2.5\ln\left(2e/D_h\right) + 2.5\right\} \tag{9}$$

For the Prandtl number = 0.7 of the present study, the relationship of $G(e^+)$ with p/e, e/D_h, β, N, and e^+ for the fully rough region obtained using multi-dimensional regression analysis can be represented as:

$$G\left(e^+\right) = \left\{\left[3.0104\left(e^+\right)^{0.24064}\,(\beta)^{0.11407}\right] / \left[(N)^{0.18847}\,(p/e)^{0.073367}\,(\Lambda)^{0.13406}\right]\right\} \tag{10}$$

The deviation of Eq. (10) is ± 15% for 99% of the data.

The friction factor f and the Stanton number St_{2r} for the VG walls can be obtained from Eqs. (6) and (9), respectively, after $R(e^+)$ and $G(e^+)$ are correlated experimentally as in Eqs. (8b) and (10).

The deviation between experimental values and values estimated from proposed correlations for rough wall Nusselt number and friction factor is shown in Fig. 17. The correlations developed for Nu and f are valid for:

- Square duct with Delta wings on two opposite walls
- N = 1 and 2, for 8000 < Re < 24000, 0.1 < e/D_h < 0.5, 1.6 < p/e < 16, and 1.6 < Λ < 15

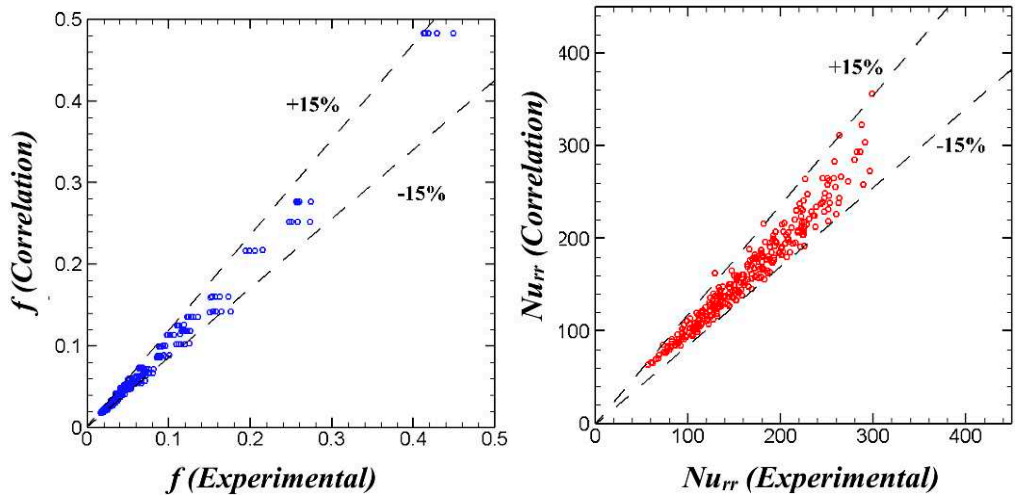

FIG. 17: Deviation between experimental values and values estimated from proposed correlations for f and Nu_{rr}

4. SUMMARY AND CONCLUSIONS

Heat transfer coefficient and pressure drop data have been presented for flow in a square channel with inline arrangement of delta wing VGs on two opposite walls of the duct for several values of the non-dimensional pitch (p/e), height (e/D_h), and aspect ratio (Λ). The heat transfer coefficients vary significantly in the spanwise and axial directions and enhanced values were observed both underneath as well as the downstream regions of the VGs. The highest heat transfer coefficients occur close to the base of the VG for all cases studied. The heat transfer coefficients on the adjacent smooth walls are comparable but slightly less than the values for the roughened walls. The highest values of the Nusselt number ratio at constant pumping power ($\mathrm{Nu}_{rr}/\mathrm{Nu}_c$) was 2.8 for the N = 1 and 3.1 for the N = 2 cases. Correlations for Nu and f were developed that predict the data with an accuracy of 15%, and confidence intervals of 99% and 96%, respectively.

REFERENCES

Akbari, M.M., Murata, A., Mochizuki, S., Saito, H., and Iwamoto, K., Effects of Vortex Generator Arrangements on Heat Transfer Enhancement over a Two-Row Fin-and-Tube Heat Exchanger, *J. Enhanced Heat Transf.*, vol. **16**, no. 4, pp. 315–329, 2009.

Bekele, A., Mishra, M., and Dutta, S., Heat Transfer Augmentation in Solar Air Heater using Delta Shaped Obstacles Mounted on the Absorber Plate, *Int. J. Sustainable Energy,* vol. **32**, no. 1, pp. 53–69, 2011.

Bekele, A., Mishra, M., and Dutta, S., Performance Characteristics of Solar Air Heater with Surface Mounted Obstacles, *Energy Conversion Manag.*, vol. **85**, pp. 603–611, 2014.

Biswas, G. and Chattopadhyay, H., Heat Transfer in a Channel with in-Built Wing Type Vortex Generators, *Int. J. Heat Mass Transf.*, vol. **35**, no. 4, pp. 803–814, 1992.

Biswas, G., Torii, K., Fuji, D., and Nishino, K., Numerical and Experimental Determination of Flow Structure and Heat Transfer Effects of Longitudinal Vortices in a Channel Flow, *Int. J. Heat Mass Transf.*, vol. **39**, no. 16, pp. 3441–3451, 1996.

Caliskan, S., Experimental Investigation of Heat Transfer in a Channel Flow with New Winglet-Type Vortex Generators, *Int. J. Heat Mass Transf.*, vol. **78**, pp. 604–614, 2014.

Chamoli, S., Lu, R., and Yu, P., Thermal Characteristic of Turbulent Flow through a Circular Tube Fitted with Perforated Vortex Generator Inserts, *Appl. Thermal Eng.*, vol. **121**, pp. 1117–1134, 2017.

Edwards, F.J. and Alker, C.J.R., The Improvement of Forced Convection Surface Heat Transfer using Protrusions in the Form of Cubes and Vortex Generators, *Proc. 5th Int. Heat Trans. Conf.*, JSME, Tokyo, vol. **2**, no. 3, pp. 244–248, 1974.

Eiamsa-Ard, S. and Promvonge, P., Influence of Double-Sided Delta-Wing Tape Insert with Alternate-Axes on Flow and Heat Transfer Characteristics in a Heat Exchanger Tube, *Chinese J. Chem. Eng.*, vol. **19**, no. 3, pp. 410–423, 2011.

Fiebig, M., Brockmeier, U., Mitra, N.K., and Guntermann, T., Structure of Velocity and Temperature Fields in Laminar Channel Flows with Longitudinal VGs, *Numer. Heat Trans., Part A*, vol. **15**, pp. 281–302, 1989.

Fiebig, M., Kallweit, P., and Mitra, N.K., Wing Type Vortex Generators for Heat Transfer Enhancement, *Proc. 8th Int. Heat Trans. Conf.*, New York: Hemisphere, vol. **6**, pp. 2909–2913, 1986.

Fiebig, M., Kallweit, P., Mitra, N.K., and Tiggelbeck, S., Heat Transfer Enhancement and Drag by Longitudinal Vortex Generators in Channel Flow, *Exp. Thermal Fluid Sci.*, vol. **4**, pp. 103–114, 1991.

Fiebig, M., Valencia, A., and Mitra, N.K., Wing-Type Vortex Generators for Fin-and-Tube Heat Exchangers, *Exp. Thermal Fluid Sci.*, vol. **7**, pp. 287–295, 1993.

Gentry, M.C. and Jacobi, A.M., Heat Transfer Enhancement by Delta-Wing Generated Tip Vortices in Flat-Plate and Developing Channel Flows, ASME *J. Heat Transf.*, vol. **124**, pp. 1158–1168, 2002.

Gentry, M.C. and Jacobi, A.M., Heat Transfer Enhancement by Delta-Wing Vortex Generators on a Flat Plate: Vortex Interactions with the Boundary Layer, *Exp. Thermal Fluid Sci.*, vol. **14**, pp. 231–242, 1997.

Gnielinski, V., New Equations for Heat Transfer and Mass Transfer in Turbulent Pipe and Channel Flow, *Int. Chem. Eng.*, vol. **16**, no. 2, pp. 359–368, 1976.

Han, J.C. and Park, J.S., Developing Heat Transfer in Rectangular Channels with Rib Turbulator, *Int. J. Heat Mass Transf.*, vol. **31**, no. 1, pp. 183–195, 1988.

Han, J.C., Heat Transfer and Friction in Channels with Two Opposite Rib-Roughened Walls, *ASME J. Heat Transf.*, vol. **106**, no. 4, pp. 774–781, 1984.

Han, J.C., Huang, J.J., and Lee, C.P., Augmented Heat Transfer in Square Channels with Wedge-Shaped and Delta-Shaped Turbulence Promoters, *J. Enhanced Heat Transf.*, vol. **1**, no. 1, pp. 37–52, 1994.

Hu, W., Su, M., Wang, L., Zhang, Q., Chang, L., Liu, S., and Wang, L., The Optimum Spacing of Circular Bank Fin Heat Exchanger with Vortex Generator, *Heat Mass Transf.*, vol. **49**, no. 9, pp. 1271–1285, 2013.

Jacobi, A.M. and Shah, R.K., Heat Transfer Surface Enhancement through the Use of Longitudinal Vortices: A Review of Recent Progress, *Exp. Thermal Fluid Sci.*, vol. **11**, pp. 295–303, 1995.

Joardar, A. and Jacobi, A.M., Impact of Leading Edge Delta-Wing Vortex Generators on the Thermal Performance of a Flat Tube, Louvered-Fin Compact Heat Exchanger, *Int. J. Heat Mass Transf.*, vol. **48**, pp. 1480–1493, 2005.

Lei, Y., Zheng, F., Song, C., and Lyu, Y., Improving the Thermal Hydraulic Performance of a Circular Tube using Punched Delta Winglet Vortex Generators, *Int. J. Heat Mass Transf.*, vol. **111**, pp. 299–311, 2017.

Lemenand, T., Habchi, C., Valle, D.D., and Peerhossaini, H., Vorticity and Convective Heat Transfer Downstream of a Vortex Generator, *Int. J. Thermal Sci.*, vol. **125**, pp. 342–349, 2018.

Liou, T., Chen, C., and Tsai, T., Heat Transfer and Fluid Flow in a Square Duct with 12 Different Shaped Vortex Generators, *ASME J. Heat Transf.*, vol. **122**, pp. 327–335, 2000.

Nalawade, M., Heat Transfer Enhancement in Ducts with Delta Wing Vortex Generators, PhD thesis, Indian Institute of Technology Bombay, 2007.

Qi, C., Min, C., Xie, S., and Kong, X., Experimental Study of Fluid Flow and Heat Transfer in a Rectangular Channel with Novel Longitudinal Vortex Generators, *J. Enhanced Heat Transf.*, vol. **17**, no. 4, pp. 301–311, 2010.

Singh, P. and Ekkad, S., Experimental Study of Heat Transfer Augmentation in a Two Pass Channel Featuring V-Ribs and Cylindrical Dimples, *Appl. Thermal Eng.*, vol. **116**, pp. 205–216, 2017.

Skullong, S. and Promvonge, P., Experimental Investigation on Turbulent Convection in Solar Air Heater Channel Fitted with Delta Winglet Vortex Generator, *Chinese J. Chem. Eng.*, vol. **22**, no. 1, pp. 1–10, 2014.

Skullong, S., Promvonge, P., Jayranaiwachira, N., and Thianpong, C., Experimental and Numerical Heat Transfer in a Tubular Heat Exchanger with Delta Wing Inserts, *Chem. Eng. Proc.: Proc. Intensif.*, vol. **109**, pp. 164–177, 2016.

Tang, L.H., Chu, W.X., Ahmed, N., and Zeng, M., A New Configuration of Winglet Vortex Generator to Enhance Heat Transfer in a Rectangular Channel, *Appl. Thermal Eng.*, vol. **104**, pp. 74–84, 2016.

Tiggelbeck, S., Mitra, N.K., and Fiebig, M., Experimental Investigations of Heat Transfer Enhancement and Flow Losses in a Channel with Double Rows of Longitudinal Vortex Generators, *Int. J. Heat Mass Transf.*, vol. **36**, no. 9, pp. 2327–2337, 1993.

Tiggelbeck, S., Mitra, N.K., and Fiebig, M., Flow Structure and Heat Transfer in a Channel with Multiple Longitudinal Vortex Generators, *Exp. Thermal Fluid Sci.*, vol. **5**, pp. 425–436, 1992.

Turk, A.Y. and Junkhan, G.H., Heat Transfer Enhancement Downstream of Vortex Generators on a Flat Plate, *Proc. 8th Int. Heat Trans. Conf.*, Hemisphere, New York, vol. **6**, pp. 2903–2908, 1986.

Wang, C.C., Lo, J., Lin, Y.T., and Wei, C.S., Flow Visualization of Annular and Delta Winglet Vortex Generators in Fin-and-Tube Heat Exchanger Application, *Int. J. Heat Mass Transf.*, vol. **45**, pp. 3803–3815, 2002a.

Wang, L.B., Zhang, Y.H., Su, Y.X., and Gao, S.D., Local and Average Heat/Mass Transfer over a Flat Tube Bank Fin Mounted In-Line Vortex Generators with Small Longitudinal Spacing, *J. Enhanced Heat Transf.*, vol. **9**, no. 2, pp. 77–87, 2002b.

Webb, R.L. and Eckert, E.R.G., Application of Rough Surfaces to Heat Exchanger Design, *Int. J. Heat Mass Transf.*, vol. **15**, pp. 1647–1658, 1972.

Wu, J.M. and Tao, W.Q., Effect of Longitudinal Vortex Generator on Heat Transfer in Rectangular Channels, *Appl. Thermal Eng.*, vol. **37**, pp. 67–72, 2012.

Xu, Z., Han, Z., Wang, J., and Liu, Z., The Characteristics of Heat Transfer and Flow Resistance in a Rectangular Channel with Vortex Generators, *Int. J. Heat Mass Transf.*, vol. **116**, pp. 61–72, 2018.

Zhu, J.X., Mitra, N.K., and Fiebig, M., Effects of Longitudinal Vortex Generators of Heat Transfer and Flow Loss in Turbulent Channel Flows, *Int. J. Heat Mass Transf.*, vol. **36**, no. 9, pp. 2339–2347, 1993.